A finite element formulation for nanoscale resonant mass sensing using the surface Cauchy–Born model

Geng Yun, Harold S. Park *

Department of Civil and Environmental Engineering, Vanderbilt University, Nashville, TN 37235, United States

Abstract

The purpose of this work is to develop the theoretical basis needed to study nanoscale resonant mass sensing with finite elements using the surface Cauchy–Born (SCB) model. The theory is developed in 1D, where it is identified that the primary modeling issue lies in capturing inhomogeneous surface stresses arising from adsorbate/substrate interactions. By utilizing internal degrees of freedom within the SCB framework, we show that the SCB model can represent the bonding energies, and thus the inhomogeneous surface stress that arises due to interactions by atoms of dissimilar materials. A key outcome of this is that it is shown that a finite element solution using the SCB model is able to simultaneously capture both mass and stiffness variations due to adsorbate/substrate interactions, and their effects on the nanostructure resonant properties. We first verify that the SCB model accurately captures the resonant properties of monatomic 1D atomic chains, then demonstrate the approach by studying the resonant properties of 1D atomic chains that interact with adsorbates. Importantly, we demonstrate that a finite element solution using the SCB model can predict the distinct shifts in resonant frequency that occur due to the adsorption of different materials on the 1D monatomic chain.
© 2008 Elsevier B.V. All rights reserved.

Keywords: Surface Cauchy–Born; Resonance; Mass sensing; Finite elements; Surface stress

1. Introduction

Nanowires have been studied intensely in recent years due to their unique and often superior mechanical, electrical and optical properties that arise because of their nanometer size scale [1–3]. Because of these unique properties, nanowires will be utilized as structural materials, bio-sensors, force and mass detectors, as circuitry and interconnects in future nanoscale devices, and as the basic building blocks of nanoelectromechanical systems (NEMS) [4–8].

Nanowires are structurally unique because they have a relatively large ratio of surface area to volume, particularly when compared to larger bulk materials. Because surface atoms have a different bonding environment than atoms that lie within the material bulk, the elastic properties of surfaces differ from those of an idealized bulk material, and the effects of the difference between surface and bulk elastic properties become magnified as the surface area to volume ratio increases with decreasing structural size [9–18].

Traditional continuum models fail to capture the size-dependent elastic properties and behavior of nanomaterials because they do not capture nanoscale free surface effects such as surface stresses [19,20], which arise because atoms at the surfaces of a material have fewer bonding neighbors than those that lie within the bulk. Therefore, researchers have focused on developing enhanced continuum models that strive to capture the non-bulk elastic behavior of nanomaterials [19,21–31]. A common thread that connects some of the above works [23,26,27] is that they are based on modifications to the surface elasticity formulation of Gurtin and Murdoch [21], in which a surface stress tensor is introduced to augment the bulk stress tensor typically utilized in continuum mechanics. A complicating factor

---

* Corresponding author. Tel.: +1 303 492 7750.
  E-mail address: harold.park@colorado.edu (H.S. Park).

in this formulation is due to the presence of the surface stress, which creates a coupled system of equations with non-standard boundary conditions. The solution of the coupled field equations combined with the non-classical boundary conditions makes the application of this theory to generalized nanomechanical boundary value problems a challenging task.

Computational modeling of the mechanics of nanomaterials have recently occurred through the development of multiple scale methods, which ideally combine the insights into the detailed response of materials that are available through atomistics with the reduced computational expense that continuum approaches offer [32–45]; excellent reviews of multiple scale modeling are those of Liu et al. [46] and Curtin and Miller [47]. However, with few exceptions [35,30], these methods are incapable of capturing atomic-scale surface stress effects, which precludes the possibility of utilizing these approaches to study and design nanowire-based NEMS devices.

Recently, the surface Cauchy–Born (SCB) model was developed by Park and co-workers to capture surface stress effects on nanomaterials within a continuum mechanics framework [48,49]. The SCB extends the traditional bulk Cauchy–Born (BCB) theory [32] by augmenting the continuum bulk energy density with a surface energy density that enables it to capture nanoscale surface stress effects. The SCB model is advantageous as it enables the solution of three-dimensional nanomechanical boundary value problems including surface stress effects using traditional non-linear finite element (FE) methods; this makes it computationally tractable, particularly for large systems, that direct atomistic simulations cannot model. In addition, many of the well-developed advantages of FE calculations, including automated meshing for arbitrary geometries, non-linear solution methodologies, ease and choice of boundary condition imposition, are directly applicable for the solution of nanomechanical boundary value problems.

In the present work, we further develop the SCB model to capture adsorbate/substrate interactions with the goal of modeling nanoscale resonant mass sensing. Low-dimensional nanostructures, such as nanowires, are viewed as optimal materials for mass sensing due to their combination of high strength and low weight. For example, recent research [50] has indicated that detection on the scale of individual molecules ($\approx 10^{-21}$ g) should be possible in the near future with nanowire-based NEMS. Because of their low weight, nanowires are extremely sensitive to adsorbed mass, which is detected by determining the shift in the nanowire resonant frequency that occurs due to the added mass.

Because the resonant frequency can be written as $\omega_0 = \sqrt{k/m}$, where k is the nanowire stiffness and m is the mass, changes in the resonant frequency can be directly related to the amount of mass adsorbed if the stiffness k remains constant. However, mass adsorption generally leads to bending and deflection of the nanowire due to vari-

ations in surface stress arising from adsorbate/substrate interactions; recent experimental and theoretical work [51] has shown that while added mass is expected to *decrease* the resonant frequencies of nanocantilevers, the corresponding change in stiffness due to the mass adsorption can actually *increase* the resonant frequency, leading to confusion in determining the molecule or atom that has been adsorbed.

A variety of analytic models have been developed to study the effects of added mass on the resonant properties of nanowires [52–56]. The analytic models, while elegant, do not enable a generalized design framework to optimize the resonant sensitivity of the nanowires in three-dimensions, and do not account for surface stress effects on the elastic properties of the substrate nanowires, which leads to incorrect resonant frequency predictions due to the inability to account for the size-dependence in nanowire elastic properties [57]. Furthermore, because the adsorbed atoms are generally a different species than the sensing nanowire, the issue of modeling the inhomogeneous surface stresses and their effects on the nanowire stiffness that arise due to the interactions of dissimilar materials must be accounted for.

The purpose of the present work is therefore to establish, in 1D, the theoretical framework needed to study nanoscale resonant mass sensing with finite elements using the SCB model. We accomplish this in the present work through the incorporation of internal degrees of freedom within the surface clusters that are utilized in the SCB model, and show that the SCB with internal degrees of freedom can represent the inhomogeneous surface deformation that occurs due to the adsorbed atom; importantly, variations in both mass and stiffness due to the adsorbed atom are captured within the SCB approach. The utilization of the internal degrees of freedom makes this one of the first works to model the interaction of different material species within the Cauchy–Born framework. 1D numerical examples using the finite element method in conjunction with the SCB model demonstrate the predictive ability of the SCB model to distinguish, through distinct shifts in resonant frequency, between different materials adsorbing on monatomic 1D atomic chains as compared to benchmark fully atomistic calculations.

2. Surface Cauchy–Born model

2.1. Motivation

To motivate the development of the SCB model, we first demonstrate the importance of accounting for surface effects on the mechanical properties of nanomaterials. While many discussions about surface stresses, their mathematical definitions and other nuances are readily available in the literature [19,20], we seek to motivate the importance of surface stress effects through example.

As discussed in Section 1, atoms at free surfaces have fewer bonding neighbors than atoms lying within the mate-

rial bulk; this is illustrated in Fig. 1. The effective result of this is that the surface atoms are not in an energy minimizing configuration, as they exist at an energy configuration that is elevated with respect to the atoms within the bulk. Therefore, when nanostructures are fabricated by cutting them out of bulk materials or thin films, they are not in equilibrium. The fact that surface effects become more dominant as materials become smaller can be generically interpreted by the fact that the surface area to volume ratio, or the percentage of atoms lying at the surfaces of a structure, increases with decreasing structural size.

The physical behavior of nanostructures that are not in equilibrium due to surface effects is shown in Fig. 2, which illustrates the behavior of a ⟨100⟩ gold nanowire modeled using an embedded atom (EAM) potential [58] created with atoms placed in positions corresponding to a bulk, undeformed lattice. The initial nanowire length was 15.9 nm, while the square cross section had length 2.5 nm. As the atoms in Fig. 2 are colored by their potential energy, it is
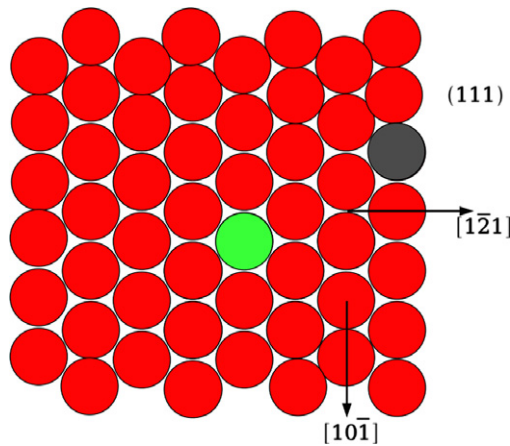
noteworthy that the potential energy of the atoms at the surface (−2.76 eV, −3.06 eV, −3.35 eV) are *greater* than those of the atoms within the bulk (−3.93 eV).

Due to the presence of the surface atoms, the initial configuration of the nanowire is not an energy minimizing one, so the nanowire *elastically* contracts nearly 5% due to the surface stresses. At equilibrium, the tensile stress of the surfaces is balanced by the compressive state that exists in the nanowire core [59]. The contraction of the nanowires is physically understandable, as that leads to the surface atoms acquiring more bonding neighbors and a higher electron density, which leads to a lower energy and more stable configuration.

In general, as the nanowire is made larger, the amount of compressive relaxation strain it undergoes due to the surface stresses decreases until the bulk limit is eventually reached, and no observable relaxation occurs. In contrast, if the nanowire cross section is made smaller, the surface stresses may become sufficient to drive reversible phase transformations and reorientations to other, lower energy configurations [60–62] that lead to shape memory and pseudoelastic properties. The critical point to emphasize here is that the surface stresses are capable of causing unusual and unique nanoscale mechanical behavior and phenomena that are not observed in the corresponding bulk material.

2.2. Overview

The theoretical basis for the SCB model was developed in earlier works [48,49]; thus, we briefly overview the major ideas in this section.

The CB model is based on Green elastic theory, in which continuum stress and moduli are derived assuming the existence of a strain energy density function Φ. In order to satisfy material frame indifference, the strain energy density Φ must be expressed as a function of the right stretch tensor

Fig. 1. Illustration of bulk (green) and surface (grey) atoms on the {111} plane of an FCC crystal. (For interpretation of the references to colour in this figure legend, the reader is referred to the web version of this article.)
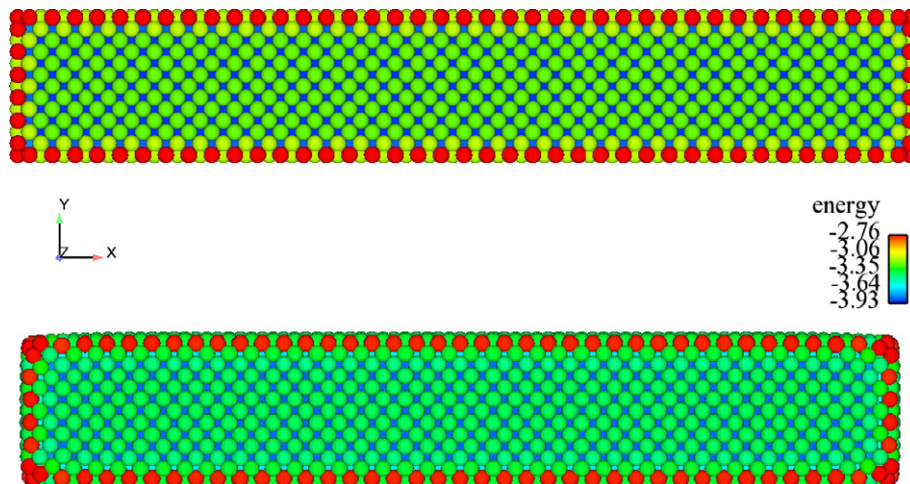
Fig. 2. Top: initial, non-equilibrium configuration of a ⟨100⟩ gold nanowire. Bottom: final, energy minimizing configuration of the nanowire at 5% elastic compressive strain.

C, i.e. $\Phi(\mathbf{C})$, where $\mathbf{C} = \mathbf{F}^{\mathrm{T}}\mathbf{F}$ and $\mathbf{F}$ is the continuum deformation gradient.

To create a link between atomistics and continua, the strain energy density can be constructed for crystalline materials by considering the bonds in a representative volume of the crystal [32,63]. For the case of a centrosymmetric crystal modeled using only pair interactions, the strain energy density is defined in terms of the interatomic potential U as [63]:

$$\Phi(\mathbf{C}) = \frac{1}{2}\frac{1}{\Omega_0^{\mathrm{a}}}\sum_{i=1}^{n_{\mathrm{b}}} U(r^{(i)}(\mathbf{C})). \qquad (1)$$

In (1), n_{b} is the total number of bonds to a representative bulk atom, Ω_0^{a} is the representative atomic volume in the undeformed configuration and $r^{(i)}$ is the deformed bond length, which follows the relationship:

$$r^{(i)} = \sqrt{\mathbf{R}_0^{(i)} \cdot \mathbf{C}\mathbf{R}_0^{(i)}}, \qquad (2)$$

where $\mathbf{R}_0$ is the undeformed bond vector. From the strain energy density given in (1), one can obtain standard continuum stress measures such as the second Piola–Kirchoff stress ($\mathbf{S}$) as

$$\mathbf{S}(\mathbf{C}) = 2\frac{\partial \Phi(\mathbf{C})}{\partial \mathbf{C}} = \frac{1}{\Omega_0^{\mathrm{a}}}\sum_{i=1}^{n_{\mathrm{b}}}\left(U'(r^{(i)})\frac{\partial r^{(i)}}{\partial \mathbf{C}}\right). \qquad (3)$$

The strain energy density (1) is exact in describing the change in energy per volume of a bulk atom in a corresponding defect-free atomistic system subject to homogeneous deformation. Furthermore, the continuum stress measure in (3) is derived using atomistic information; thus the CB hypothesis is said to be hierarchically multiscale in nature. We note that the CB model can also be utilized in conjunction with more complicated interatomic interactions such as embedded atom (EAM) potentials [64,32,49] for FCC metals, Tersoff-type potentials for silicon [65,66], or carbon nanotubes [67,68].

There are two major assumptions underlying the CB hypothesis. The first is that, as mentioned above, the underlying atomistic system is constrained to deform homogeneously according to the stretch tensor $\mathbf{C}$. This restriction can be relaxed, for example through development of the quasicontinuum, or non-local CB model [32]. The second major assumption is that all points at which the Cauchy–Born hypothesis is applied are assumed to lie in the bulk because $\Phi(\mathbf{C})$ does not account for surface effects. Therefore, in order to capture nanoscale free surface effects such as surface stresses, we will augment the bulk energy density in (1) with a surface energy density which accounts for the non-bulk potential energy that atoms lying along the surfaces of a body exhibit.

2.3. Surface energy densities

In this section, we discuss the methodology by which the total atomistic potential energy of a body is represented by continuum energy densities with appropriate representations for bulk and surface energy densities. The relationship between the continuum strain energy and the atomistically calculated potential energy of the fixed/free 1D chain illustrated in Fig. 3 can be written as

$$\sum_{\alpha=1}^{n_{\mathrm{atoms}}} U_\alpha(r) \approx \int_{\Omega_0^{\mathrm{bulk}}} \Phi(C)\,\mathrm{d}\Omega + \int_{\Gamma_0^1} \Gamma_1(C)\,\mathrm{d}\Gamma$$
$$+ \int_{\Gamma_0^2} \Gamma_2(C)\,\mathrm{d}\Gamma + \int_{\Gamma_0^{\mathrm{na}}} \Gamma_{\mathrm{na}}(C)\,\mathrm{d}\Gamma$$
$$+ \int_{\Gamma_0^{\mathrm{na}-1}} \Gamma_{\mathrm{na}-1}(C)\,\mathrm{d}\Gamma, \qquad (4)$$

where U_α is the potential energy of atom α, r is the interatomic distance, $\Phi(C)$ is the bulk strain energy density, Ω_0^{bulk} represents the volume of the body in which all atoms are fully coordinated, $\Gamma_1(C)$ is the surface energy density of atom 1, $\Gamma_2(C)$ is the surface energy density of atom 2, $\Gamma_{\mathrm{na}}(C)$ is the surface energy density of atom na, $\Gamma_{\mathrm{na}-1}(C)$ is the surface energy density of atom na $- 1$, Γ_0 represents the surface area of the body in which the atoms are undercoordinated and n_{atoms} is the total number of atoms in the system.

We emphasize that the number of surface integrals in (4) is solely dictated by the range of the interatomic potential; the range of the interatomic potential dictates the number of atomic layers at or near the surface which do not interact with a full complement of atomic neighbors.

The surface energy densities $\Gamma(C)$ represent the energy per unit *area* for atoms lying at or near the surfaces of a material; the energy is different for these atoms due to the fact that they have fewer bonding neighbors as compared to an atom lying within the material bulk. The surface energy density for a given atom at or near the surface can be generally written as

$$\Gamma_i(\mathbf{C}) = \frac{1}{2}\frac{1}{\Gamma_0^i}\sum_{j=1}^{n_{\mathrm{b}_i}} U(r^{(j)}(\mathbf{C})), \qquad (5)$$

where n_{b_i} is the number of bonds for atoms in surface layer i and Γ_0^i is the representative area of an atom lying in surface layer i. The surface atoms in Fig. 3 for which the surface energy densities in (5) are calculated explicitly are termed surface clusters; further details on the surface clusters can be found in Park et al. [48].

The surface energy density as written in (5) is valid for FCC lattices, or lattices which have one atom per surface unit cell. For alloyed systems or lattices such as graphene which will require more than one atom per surface unit cell, additional kinematic, or internal degrees of freedom must
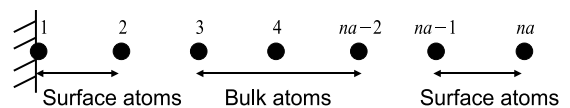
Fig. 3. Illustration of bulk and surface atoms for a fixed/free 1D atomic chain with second nearest neighbor interactions.

be introduced. These modifications have been made in previous Cauchy–Born extensions [65,67], and can be similarly incorporated into the present work. However, we will concentrate here on lattices that contain one atom per surface unit cell.

We can immediately define the surface stress on an atom in surface layer i resulting from the surface energy density in (5) as

$$\widetilde{\mathbf{S}}_i(\mathbf{C}) = 2\frac{\partial \Gamma_i(\mathbf{C})}{\partial \mathbf{C}} = \frac{1}{\Gamma_0^i}\sum_{j=1}^{n_{b_i}}\left(U'(r^{(j)})\frac{\partial r^{(j)}}{\partial \mathbf{C}}\right). \quad (6)$$

While the significance of the surface stress will be discussed later, the key idea is that nanoscale free surface effects, which become significant as the surface area to volume ratio of nanomaterials increases, are captured succinctly within a continuum stress measure.

3. Finite element formulation

In this section, we derive the variational formulation in 1D from which the finite element (FE) equilibrium equations can be obtained. We begin with the total potential energy of the system, which is obtained by subtracting the work due to external tractions $\mathbf{T}$ from (4) to give

$$\Pi(\mathbf{u}) = \int_{\Omega_0^{\text{bulk}}}\Phi(C)\,\mathrm{d}\Omega + \int_{\Gamma_0^1}\Gamma_1(C)\,\mathrm{d}\Gamma + \int_{\Gamma_0^2}\Gamma_2(C)\,\mathrm{d}\Gamma$$
$$+ \int_{\Gamma_0^{\text{na}}}\Gamma_{\text{na}}(C)\,\mathrm{d}\Gamma + \int_{\Gamma_0^{\text{na}-1}}\Gamma_{\text{na}-1}(C)\,\mathrm{d}\Gamma - \int_{\Gamma_0}(\mathbf{T}\cdot\mathbf{u})\,\mathrm{d}\Gamma. \quad (7)$$

In order to obtain a form suitable for FE calculations, we introduce the standard discretization of the displacement field $\mathbf{u}(\mathbf{X})$ using FE shape functions as

$$\mathbf{u}(\mathbf{X}) = \sum_{I=1}^{nn} N_I(\mathbf{X})\mathbf{u}_I, \quad (8)$$

where N_I are the shape or interpolation functions, nn are the total number of nodes in the discretized continuum, and $\mathbf{u}_I$ are the displacements of node I [69]. Substituting (8) into (7) and differentiating gives the minimizer of the potential energy and also the FE nodal force balance [69]

$$\frac{\partial \Pi}{\partial \mathbf{u}_I} = \int_{\Omega_0^{\text{bulk}}}\mathbf{B}^{\text{T}}SF^{\text{T}}\,\mathrm{d}\Omega + \int_{\Gamma_0^1}\mathbf{B}^{\text{T}}\widetilde{S}^{(1)}F^{\text{T}}\,\mathrm{d}\Gamma$$
$$+ \int_{\Gamma_0^2}\mathbf{B}^{\text{T}}\widetilde{S}^{(2)}F^{\text{T}}\,\mathrm{d}\Gamma + \int_{\Gamma_0^{\text{na}}}\mathbf{B}^{\text{T}}\widetilde{S}^{(\text{na})}F^{\text{T}}\,\mathrm{d}\Gamma$$
$$+ \int_{\Gamma_0^{\text{na}-1}}\mathbf{B}^{\text{T}}\widetilde{S}^{(\text{na}-1)}F^{\text{T}}\,\mathrm{d}\Gamma - \int_{\Gamma_0}N_I\mathbf{T}\,\mathrm{d}\Gamma, \quad (9)$$

where S is the second Piola–Kirchoff stress due to the bulk strain energy, $\mathbf{B}^{\text{T}} = (\frac{\partial N_I}{\partial \mathbf{X}})^{\text{T}}$ and $\widetilde{S}^{(i)}$ are surface stresses, similar to (6) and of the form

$$\widetilde{S}^{(i)}(C) = \frac{1}{\Gamma_0^{a_i}}\sum_{j=1}^{n_{b_i}}\left(U'(r^{(j)})\frac{\partial r^{(j)}}{\partial C}\right). \quad (10)$$

In (10), $\Gamma_0^{a_i}$ represents the normalizing area for atomic layer i, and n_{b_i} represents the number of bonds for an atom lying within atomic layer i, which may differ depending on whether the atom lies on the first or second layer of surface atoms.

The key idea in (9) is that the FE internal forces arise from integrals that have either a volume or surface area dependence. Therefore, as materials become smaller and their surface area to volume ratio increases, the surface integrals and thus the surface stress terms will become critical in capturing size and surface effects. In contrast, for larger, more bulk-like materials, the volume terms will dominate the surface terms, and the model degenerates to a bulk Cauchy–Born model with increasing size.

4. Extension of SCB model for nanoscale resonant mass sensing

4.1. Motivation: 1D monatomic chain

In this section, we motivate the need for internal degrees of freedom for the surface clusters by showing numerical examples involving both monatomic 1D chains, as well as chains of atoms that interact with single adsorbate atoms. We first consider a 1D monatomic chain of na = 61 atoms that is fixed at the left end and free at the right end, as illustrated in Fig. 4. The chain of atoms is modeled using a Lennard–Jones (LJ) potential, which takes the form:

$$U(r) = 4\epsilon\left(\left(\frac{\sigma}{r}\right)^{12} - \left(\frac{\sigma}{r}\right)^{6}\right) \quad (11)$$

where ϵ has units of energy and σ has units of length. We utilized LJ parameters for copper (Cu) [70], where $\epsilon = 0.415$ eV and $\sigma = 2.277$ Å, while considering nearest and second nearest neighbor interactions for each atom. Note that because of the second nearest neighbor interactions, the 1D chain is initially not in equilibrium due to surface stresses, and the chain relaxes as a result. No external forces are applied at any point in the simulations; all deformations are caused by the surface stresses. A molecular statics (MS) calculation was performed to find the energy minimizing positions of the atoms due to the surface stresses.

The 1D chain of atoms was also discretized using 10 finite elements for the SCB calculation. It is found that in the MS simulation, the displacement of the last copper atom on the right end of the chain due to surface stresses is 0.00646 Å. In the SCB simulation, the relaxation of the
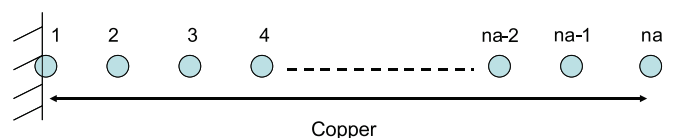
Fig. 4. 1D fixed/free chain of copper atoms.

right most node is 0.00644 Å, which indicates that the SCB model accurately captures the relaxation of a 1D monatomic chain. Note that the expansion of the 1D chain is an anomaly that can be attributed to the inability of the LJ potential to capture environment-dependent bonding at the surfaces; such effects are well captured for FCC metals by EAM potentials, and are naturally transferred to the corresponding SCB models [49].

4.2. Internal degrees of freedom for adsorbate/substrate interactions

To examine the inability of the standard SCB model to capture adsorbate effects on the minimum energy configurations of 1D atomic chains, we utilize the same fixed/free chain comprised of 61 Cu atoms, while adding a single adsorbate (silver or nickel) atom to the right-hand side of the chain as illustrated in Fig. 5; the adsorbate atom is taken to constitute the new surface. For both the silver (Ag) and nickel (Ni) atoms, we utilize parameters given in Agrawal et al. [70] to be $\epsilon_{Ag} = 0.351$ eV and $\sigma_{Ag} = 2.574$ Å, $\epsilon_{Ni} = 0.529$ eV and $\sigma_{Ni} = 2.22$ Å; nickel was chosen because it has a larger difference in ϵ with Cu than does Ag. The Cu–adsorbate mixed bond interactions are determined using the averaging approach given in Guan et al. [71]

$$\epsilon^{mix} = \sqrt{\epsilon_s + \epsilon_a}, \quad \sigma^{mix} = \left(\frac{\sigma_s + \sigma_a}{2}\right), \quad (12)$$

where s and a represent substrate (Cu) and adsorbate atoms (Ag or Ni), respectively.

The result of the MS (61 Cu and 1 Ag adsorbate atom) calculation is that the displacement of the right most Ag atom is 0.172 Å; in contrast, the SCB simulation using 10 finite elements predicts a displacement of the right most node of 0.246 Å, which indicates that the presence of the adsorbate Ag atom is the reason for the inaccuracy in the SCB calculation. For the case with the Ni adsorbate, the MS predicts a relaxation of −0.0257 Å, while the SCB predicts a relaxation of −0.0259 Å.

The cause for the error in the SCB model is the assumption that the underlying lattice deformation is homogeneous. Due to this assumption, the Cu atoms that interact with the adsorbate Ag atom cannot relax differently than those Cu atoms that interact only with other Cu atoms, which clearly places a non-physical constraint on the system considering that the bonding energy between Cu atoms and the adsorbate Ag atom differs from that of two Cu atoms. To alleviate this problem,

we propose the addition of internal degrees of freedom ξ_1 and ξ_2 to the Cu–adsorbate bonds, which is illustrated in Fig. 6. Because of the additional degrees of freedom given to the Cu atoms that interact with the adsorbate atom, the deformed Cu–adsorbate bond lengths can be written as

$$r_{na-3,na-1} = F \cdot (2ha - \xi_1), \quad r_{na-2,na-1} = F \cdot (ha - \xi_1), \quad (13)$$

$$r_{na-2,na} = F \cdot (2ha - \xi_2), \quad r_{na-1,na} = F \cdot (ha + \xi_1 - \xi_2),$$
$$r_{na-1,na+1} = F \cdot (2ha + \xi_1), \quad r_{na,na+1} = F \cdot (ha + \xi_2),$$

where F is the scalar deformation gradient in 1D and ha is the initial Cu–Cu bond length. To determine the two internal degrees of freedom, we minimize the total energy U_{Total} which incorporates all the bond lengths altered by the internal degrees of freedom in (13):

$$U_{Total} = 4\epsilon_s \left(\left(\frac{\sigma_s}{r_{na-3,na-1}}\right)^{12} - \left(\frac{\sigma_s}{r_{na-3,na-1}}\right)^6 \right)$$
$$+ 4\epsilon_s \left(\left(\frac{\sigma_s}{r_{na-2,na-1}}\right)^{12} - \left(\frac{\sigma_s}{r_{na-2,na-1}}\right)^6 \right)$$
$$+ 4\epsilon_s \left(\left(\frac{\sigma_s}{r_{na-2,na}}\right)^{12} - \left(\frac{\sigma_s}{r_{na-2,na}}\right)^6 \right)$$
$$+ 4\epsilon_s \left(\left(\frac{\sigma_s}{r_{na-1,na}}\right)^{12} - \left(\frac{\sigma_s}{r_{na-1,na}}\right)^6 \right)$$
$$+ 4\epsilon^{mix} \left(\left(\frac{\sigma^{mix}}{r_{na-1,na+1}}\right)^{12} - \left(\frac{\sigma^{mix}}{r_{na-1,na+1}}\right)^6 \right)$$
$$+ 4\epsilon^{mix} \left(\left(\frac{\sigma^{mix}}{r_{na,na+1}}\right)^{12} - \left(\frac{\sigma^{mix}}{r_{na,na+1}}\right)^6 \right) \quad (14)$$

By differentiating U_{Total} in (14) with respect to ξ_1 and ξ_2, we obtain a two-component non-linear system; the solution to the non-linear system can be obtained using Newton's method which gives ξ_1 and ξ_2 for a given F.
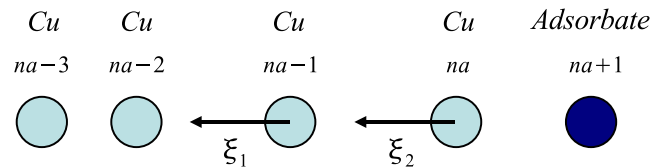
Fig. 6. Illustration of internal degrees of freedom for surface cluster atoms.
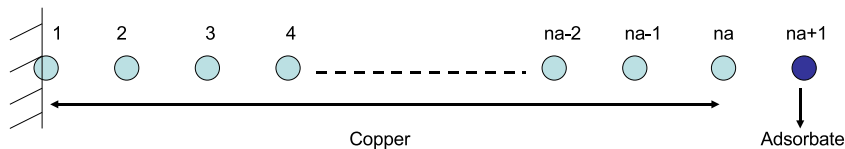
Fig. 5. 1D fixed/free chain of copper atoms with an adsorbate atom at the free end.

After obtaining ξ_1 and ξ_2, we can calculate the strain energy densities Γ_{na-2}, Γ_{na-1}, Γ_{na} and Γ_{na+1} using (5); the associated surface stress for each surface cluster is then found using (6). The additional surface clusters are required to account for the long-range influence of the adsorbate atom on the displacement field of the substrate copper atoms. Accounting for all surface clusters leads to a total potential energy of the form, correlating to Fig. 5

$$\Pi(\mathbf{u}) = \int_{\Omega_0^{bulk}} \Phi(C)\,d\Omega + \int_{\Gamma_0^1} \Gamma_1(C)\,d\Gamma + \int_{\Gamma_0^2} \Gamma_2(C)\,d\Gamma$$
$$+ \int_{\Gamma_0^{na-2}} \Gamma_{na-2}(C)\,d\Gamma + \int_{\Gamma_0^{na-1}} \Gamma_{na-1}(C)\,d\Gamma$$
$$+ \int_{\Gamma_0^{na}} \Gamma_{na}(C)\,d\Gamma + \int_{\Gamma_0^{na+1}} \Gamma_{na+1}(C)\,d\Gamma. \quad (15)$$

We do not account for the external tractions $\mathbf{T}$ in (15) as none of the numerical examples in this work utilize externally applied forces.

Fig. 7 shows a schematic of the FE mesh, where N is the number of elements and $N+1$ is the number of nodes. The domain between the FE nodes $0'$ and N' is the bulk domain, in which the stress is calculated using the bulk energy density $\Phi(C)$, while the stresses in the domains between nodes 0 and $0'$ and N' and N are calculated from the surface energy densities $\Gamma(C)$. The non-bulk region between nodes N' and N is larger because of the presence of the adsorbate on the right side of the 1D chain.

In a typical element, e_i $(i = 1, 2, \ldots, N)$, the interpolated displacement is $u(x) = u_{i-1}\frac{x_i - x}{h} + u_i\frac{x - x_{i-1}}{h}$, where h is the length of the element, u_{i-1} and u_i are the nodal displacements and x_{i-1} and x_i are the nodal coordinates. The deformation gradient in each element is $F = 1 + \frac{u_i - u_{i-1}}{h}$, and is constant in each element as we utilized only linear, two-node finite elements. After the FEM discretization, the functional (15) can be expressed in terms of the nodal displacements u_i $(i = 1, 2, \ldots, N)$ as

$$\Pi(\mathbf{u}) = \int_{x_{0'}}^{x_1} \Phi(C)\,dx + \sum_{i=2}^{N-1} \int_{x_{i-1}}^{x_i} \Phi(C)\,dx + \int_{x_{N-1}}^{x_{N'}} \Phi(C)\,dx$$
$$+ \Gamma_1(C) + \Gamma_2(C) + \Gamma_{na-2}(C) + \Gamma_{na-1}(C) + \Gamma_{na}(C)$$
$$+ \Gamma_{na+1}(C) \quad (16)$$

The integrals for the surface energy densities Γ in (16) are not written because the area for the surface unit cells is taken to be unity in 1D. The expressions for the terms in the functional (16) are given as

$$\int_{x_{0'}}^{x_1} \Phi(C)\,dx = 4\epsilon_s(x_1 - x_{0'})\left(\frac{\sigma_s^{12}\left(\frac{1}{2^{12}}+1\right)}{ha^{13}F^{12}} - \frac{\sigma_s^6\left(\frac{1}{2^6}+1\right)}{ha^7F^6}\right) \quad (17)$$

$$\sum_{i=2}^{N-1} \int_{x_{i-1}}^{x_i} \Phi(C)\,dx = \sum_{i=2}^{N-1} 4\epsilon_s h\left(\frac{\sigma_s^{12}\left(\frac{1}{2^{12}}+1\right)}{ha^{13}F^{12}} - \frac{\sigma_s^6\left(\frac{1}{2^6}+1\right)}{ha^7F^6}\right) \quad (18)$$

$$\int_{x_{N-1}}^{x_{N'}} \Phi(C)\,dx = 4\epsilon_s(x_{N'} - x_{N-1})\left(\frac{\sigma_s^{12}\left(\frac{1}{2^{12}}+1\right)}{ha^{13}F^{12}} - \frac{\sigma_s^6\left(\frac{1}{2^6}+1\right)}{ha^7F^6}\right) \quad (19)$$

$$\Gamma_1(C) = 2\epsilon_s\left(\frac{\sigma_s^{12}\left(\frac{1}{2^{12}}+1\right)}{ha^{12}F^{12}} - \frac{\sigma_s^6\left(\frac{1}{2^6}+1\right)}{ha^6F^6}\right) \quad (20)$$

$$\Gamma_2(C) = 4\epsilon_s\left(\frac{\sigma_s^{12}\left(\frac{1}{2^{13}}+1\right)}{ha^{12}F^{12}} - \frac{\sigma_s^6\left(\frac{1}{2^7}+1\right)}{ha^6F^6}\right) \quad (21)$$

$$\Gamma_{na-2}(C) = 2\epsilon_s\left(\frac{\sigma_s^{12}\left(\frac{1}{2^{12}}+1\right)}{ha^{12}F^{12}} - \frac{\sigma_s^6\left(\frac{1}{2^6}+1\right)}{ha^6F^6}\right)$$
$$+ 2\epsilon_s\left(\frac{\sigma_s^{12}}{(ha - \xi_1)^{12}F^{12}} - \frac{\sigma_s^6}{(ha - \xi_1)^6F^6}\right)$$
$$+ 2\epsilon_s\left(\frac{\sigma_s^{12}}{(2ha - \xi_2)^{12}F^{12}} - \frac{\sigma_s^6}{(2ha - \xi_2)^6F^6}\right) \quad (22)$$

$$\Gamma_{na-1}(C) = 2\epsilon_s\left(\frac{\sigma_s^{12}}{(2ha - \xi_1)^{12}F^{12}} - \frac{\sigma_s^6}{(2ha - \xi_1)^6F^6}\right)$$
$$+ 2\epsilon_s\left(\frac{\sigma_s^{12}}{(ha - \xi_1)^{12}F^{12}} - \frac{\sigma_s^6}{(ha - \xi_1)^6F^6}\right)$$
$$+ 2\epsilon_s\left(\frac{\sigma_s^{12}}{(ha + \xi_1 - \xi_2)^{12}F^{12}} - \frac{\sigma_s^6}{(ha + \xi_1 - \xi_2)^6F^6}\right)$$
$$+ 2\epsilon^{mix}\left(\frac{(\sigma^{mix})^{12}}{(2ha + \xi_1)^{12}F^{12}} - \frac{(\sigma^{mix})^6}{(2ha + \xi_1)^6F^6}\right) \quad (23)$$

$$\Gamma_{na}(C) = 2\epsilon_s\left(\frac{\sigma_s^{12}}{(2ha - \xi_2)^{12}F^{12}} - \frac{\sigma_s^6}{(2ha - \xi_2)^6F^6}\right)$$
$$+ 2\epsilon_s\left(\frac{\sigma_s^{12}}{(ha + \xi_1 - \xi_2)^{12}F^{12}} - \frac{\sigma_s^6}{(ha + \xi_1 - \xi_2)^6F^6}\right)$$
$$+ 2\epsilon^{mix}\left(\frac{(\sigma^{mix})^{12}}{(ha + \xi_2)^{12}F^{12}} - \frac{(\sigma^{mix})^6}{(ha + \xi_2)^6F^6}\right) \quad (24)$$

Fig. 7. Spatial decomposition of bulk and non-bulk regions for FEM implementation of SCB model to capture adsorbate effects.

$$\Gamma_{\mathrm{na}+1}(C) = 2\epsilon^{\mathrm{mix}}\left(\frac{(\sigma^{\mathrm{mix}})^{12}}{(2\mathrm{ha}+\xi_1)^{12}F^{12}} - \frac{(\sigma^{\mathrm{mix}})^{6}}{(2\mathrm{ha}+\xi_1)^{6}F^{6}}\right)$$
$$+ 2\epsilon^{\mathrm{mix}}\left(\frac{(\sigma^{\mathrm{mix}})^{12}}{(\mathrm{ha}+\xi_2)^{12}F^{12}} - \frac{(\sigma^{\mathrm{mix}})^{6}}{(\mathrm{ha}+\xi_2)^{6}F^{6}}\right) \quad (25)$$

By differentiating the functional (16) with respect to the nodal displacements, we get the nodal force equilibrium, which is a multi-component non-linear system of the form

$$f_i^{\mathrm{int}} = -\frac{\partial \Pi(\mathbf{u})}{\partial u_i}, \quad i = 1, 2, \ldots, N \quad (26)$$

The corresponding tangent stiffness matrix, which is necessary for the resonant frequency calculations that we will perform later then takes the familiar form

$$K_{ij}^{\mathrm{int}} = -\frac{\partial^2 \Pi(\mathbf{u})}{\partial u_i \partial u_j} \quad (27)$$

We note that because the surface energy densities in (16) contain the effects of the Cu–adsorbate interactions, the inhomogeneous surface stresses that arise due to those interactions are transferred naturally to the continuum model through (26) and (27).

The improvement in capturing the relaxation due to the adsorbates using the internal degrees of freedom is shown in Table 1 for the Ag adsorbate case and in Table 2 for the Ni adsorbate case. As can be seen, the SCB model with internal degrees of freedom accurately captures the inhomogeneous relaxation due to adsorbate/substrate interactions. Furthermore, the relaxation is shown to converge to the exact solution obtained using MS through FEM mesh refinement; the convergence is significantly faster than observed using the SCB model without internal degrees of freedom. Finally, we note the ability of the SCB model to accurately capture either compressive or tensile surface stresses leading to either expansion, as in the case of the Ag adsorbate, or compression, as in the case of the Ni adsorbate.

We will, in the following section, use the SCB model with internal degrees of freedom to capture shifts in the res-

Table 1
Displacement of the silver adsorbate atom (in Å) due to surface stresses

MS	Elements	SCB	Error	SCB (internal DOFs)	Error
0.172	5	0.257	0.496	0.192	0.117
0.172	10	0.246	0.431	0.185	0.076
0.172	15	0.236	0.372	0.178	0.038

Table 2
Displacement of the nickel adsorbate atom (in Å) due to surface stresses

MS	Elements	SCB	Error	SCB (internal DOFs)	Error
−0.02565	5	−0.02592	0.0103	−0.02574	0.0034
−0.02565	10	−0.02589	0.0093	−0.02573	0.0029
−0.02565	15	−0.02586	0.0083	−0.02571	0.0024

onant frequencies of 1D atomic chains both with and without the influence of adsorbates.

5. 1D numerical examples: resonant frequencies

5.1. FEM resonance preliminaries

To obtain resonant frequencies for the SCB model, we solve the standard eigenvalue problem for the resonant frequencies using the FE mass and stiffness matrices. To do so, we note that the equation describing the eigenvalue problem for continuum elastodynamics is written as

$$(\mathbf{K} - \omega^2 \mathbf{M})\mathbf{u} = 0, \quad (28)$$

where $\mathbf{M}$ is the consistent FE mass matrix and $\mathbf{K}$ is the FE stiffness matrix, which can be found using (27); the stiffness matrix is derived using the LJ potential (11) along with the parameters discussed earlier. The solution of the eigenvalue problem described in (28) gives the resonant frequencies ω.

To obtain the FEM mass matrix, we first calculate the mass density as follows:

$$\rho = \frac{m_{\mathrm{Cu}}}{\mathrm{ha}} \quad (29)$$

where m_{Cu} is the mass of a copper atom and ha is the undeformed Cu–Cu bond length. The element mass matrix is

$$\mathbf{M}_{\mathrm{e}} = \int \rho \mathbf{N}^{\mathrm{T}} \mathbf{N} \, \mathrm{d}x \quad (30)$$

where $\mathbf{M}_{\mathrm{e}}$ can be written as, for elements that contain only Cu–Cu interactions

$$\mathbf{M}_{\mathrm{e}} = \begin{pmatrix} \frac{\rho h}{3} & \frac{\rho h}{6} \\ \frac{\rho h}{6} & \frac{\rho h}{3} \end{pmatrix} \quad (31)$$

where h is the length of the element. Because the adsorbate is the last atom of the 1D chain, the only element mass matrix that is impacted by the adsorbate is the last element. We account for the mass of the adsorbate atom m_{adsorb} by directly adding it to the last element mass matrix as

$$\mathbf{M}_{\mathrm{e}} = \begin{pmatrix} \frac{\rho h}{3} & \frac{\rho h}{6} \\ \frac{\rho h}{6} & \frac{\rho h}{3} + (m_{\mathrm{adsorb}} - m_{\mathrm{Cu}}) \end{pmatrix} \quad (32)$$

The resonant frequencies for the benchmark MS calculations were also found for comparison; the stiffness matrix for the MS calculation was found using (27), while the mass matrix was simply a diagonal matrix with the atomic masses on the diagonal.

5.2. Resonant frequencies of 1D fixed/free monatomic chains

We first perform a series of calculations to verify that the SCB model captures variations in the resonant frequencies of the 1D atomic chain without adsorbates. The comparison was made between the resonant frequencies as calculated using MS for the 61 atom Cu chain with fixed/free boundary conditions and the resonant frequencies cal-

culated using 10 finite elements for both the bulk CB (BCB – without surface stresses) and SCB models for copper using the LJ parameters given earlier.

The results for the first three resonant frequencies are shown in Table 3. As can be observed, both the BCB and SCB models show resonant frequencies that are quite accurate for the fundamental mode ω_0, with less accurate results (as is typical of FEM resonant calculations) for the higher order modes ω_1 and ω_2. We note that variations in resonant frequencies between BCB and SCB models are quite small due to the small surface stresses generated by the LJ potential; this is also reflected in the small amount of relaxation that the free end of the chains undergo due to the surface stresses. For example, the strain due to surface stresses for the 61 atom Cu chain is $\epsilon = 0.00646/152.96 = 0.000042$. In contrast, realistic EAM potentials predict elastic compressive strains due to surface stresses that can be on the order of several percent for FCC metal nanowires [49,60]; this was also illustrated in the present work in Fig. 2, while the effects of the finite strain on the resonant frequencies is shown in Park and Klein [57].

The mode shapes for the first three modes are also shown in Fig. 8. As can be observed, the predicted SCB mode shapes match those predicted by the MS calculation; the mode shapes match both in the order of the modes (fundamental bending, second and third order bending) and the magnitude of the displacements.

5.3. Resonant frequencies of 1D fixed/fixed monatomic chains

A further verification of the SCB model and its ability to capture resonant frequencies was conducted using a fixed/fixed 1D atomic chain comprised of 61 Cu atoms. The first three resonant frequencies found using MS, BCB and SCB are shown in Table 4. There again, the SCB model accurately captures the resonant frequencies, with greater error in the higher order modes. The disparity between the BCB and SCB results is again relatively minute; this is due to the small magnitude of the surface stresses predicted by the LJ potential, which adds a minimal amount of internal stress to the 1D chain.

The modes for the fixed/fixed 1D monatomic chain are shown in Fig. 9. As can be observed, the mode shapes and the order of the mode shapes match those expected for a fixed/fixed 1D bar or beam, in that fundamental, second and third-order bending modes are observed.

5.4. 1D resonant mass sensing: effect of adsorbates on resonant frequency

Finally, we study the variations in the resonant frequencies of the 1D Cu chain due to both single Ni and Ag adsorbate atoms. To study the effect of added adsorbates, we calculated the resonant frequencies of a 62 atom chain

Table 3
Resonant frequency comparison for the first three modes between MS, BCB and SCB for the 1D fixed/free monatomic chain; frequencies are in GHz

Mode	MS	BCB	$\frac{\omega_{bcb}}{\omega_{ms}}$	SCB	$\frac{\omega_{scb}}{\omega_{ms}}$
ω_0	693.94	700.67	1.010	700.46	1.009
ω_1	2081.37	2119.33	1.018	2118.70	1.018
ω_2	3467.47	3590.25	1.035	3589.18	1.035

Table 4
Resonant frequency comparison for the first three modes between MS, BCB and SCB for the 1D fixed/fixed monatomic chain; frequencies are in GHz

Mode	MS	BCB	$\frac{\omega_{bcb}}{\omega_{ms}}$	SCB	$\frac{\omega_{scb}}{\omega_{ms}}$
ω_0	1399.53	1405.66	1.004	1405.47	1.004
ω_1	2798.15	2846.05	1.017	2845.78	1.017
ω_2	4194.97	4356.32	1.038	4356.20	1.038
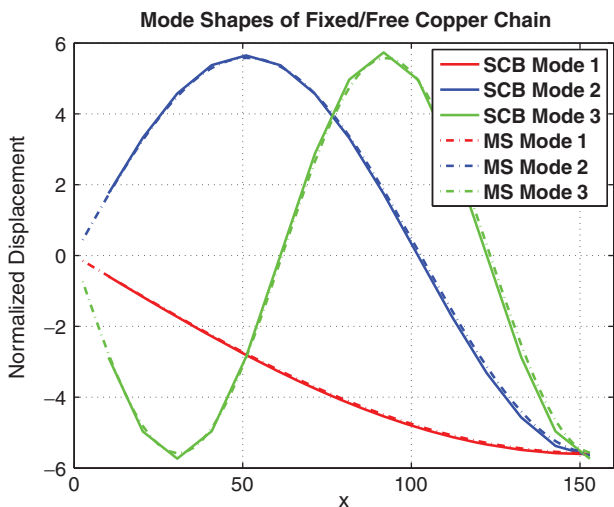
Fig. 8. First three mode shapes for fixed/free copper chain of atoms as calculated using SCB and MS simulations.
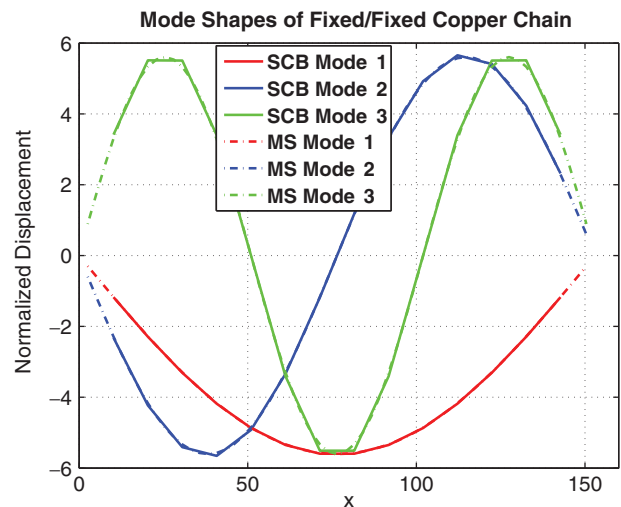
Fig. 9. First three mode shapes for fixed/fixed copper chain of atoms as calculated using SCB and MS simulations.

using MS. We utilized a 62 atom chain (the original 61 atom Cu chain plus a single adsorbate atom) because resonant mass sensing measurements are based on determining the unique change in resonant frequency that occurs for a given structure due to added mass. Because we have already quantified the resonant frequency of the 61 atom Cu chain with fixed/free boundary conditions, we can thus determine the unique shift in the fundamental mode resonant frequency that occurs due to the adsorption of both the Ni and Ag adsorbate atoms on the Cu chain. We also calculated the resonant frequencies using the SCB model with internal degrees of freedom using 10 finite elements.

The variation of the fundamental mode resonant frequencies as calculated using the SCB model for both the Ag and Ni adsorbate cases are shown in Tables 5 and 6. As can be seen, the SCB model captures well the resonant frequency with a significantly reduced number of degrees of freedom as compared to the full MS simulation; the reduction in number of degrees of freedom will be significantly larger in multiple dimensions, as has been demonstrated in previous SCB calculations that do not involve mass sensing [49]. We note also that, as would be expected, the resonant frequency including the adsorbate in Table 7 decreases as compared to the monatomic chain due to the increase in mass from the adsorbate.

The key result of this work is given in Table 7, which shows the MS and SCB predictions of the variation in resonant frequency for Ag and Ni adsorbates on the Cu chain. Table 7 shows that the adsorption of a single Ag atom on the previously monatomic 61 atom Cu chain results in a resonant frequency decrease of approximately 2.73% as calculated using a MS simulation. Importantly, the SCB model predicts a nearly identical shift in resonant frequency, a decrease of 2.76% with the adsorption of a single Ag atom.

Furthermore, the SCB model also captures the shift in resonant frequency due to adsorption of a single Ni atom on the monatomic 61 atom Cu chain. Table 7 shows that the benchmark MS calculation predicts a resonant frequency decrease of 1.5%, while the SCB model predicts a resonant frequency decrease of 1.51%. Thus, different

Table 5
Resonant frequency comparison for the fundamental mode between MS and SCB with internal degrees of freedom for the 1D fixed/free chain with a silver adsorbate atom; frequencies are in GHz

Mode	MS	SCB (internal DOFs)	$\frac{\omega_{scb}^{intdof}}{\omega_{ms}}$
ω_0	675.01	681.14	1.009

Table 6
Resonant frequency comparison for fundamental mode between MS and SCB with internal degrees of freedom for the 1D fixed/free chain with a nickel adsorbate atom; frequencies are in GHz

Mode	MS	SCB (internal DOFs)	$\frac{\omega_{scb}^{intdof}}{\omega_{ms}}$
ω_0	683.51	689.86	1.009

Table 7
Variation in resonant frequency due to nickel and silver adsorbate atoms as predicted using both MS and SCB with internal degrees of freedom

Mode	$\left(\frac{\omega_{ms}^{na}-\omega_{ms}^{a}}{\omega_{ms}^{na}}\right)_{Ag}$	$\left(\frac{\omega_{scb}^{na}-\omega_{scb}^{a}}{\omega_{scb}^{na}}\right)_{Ag}$	$\left(\frac{\omega_{ms}^{na}-\omega_{ms}^{a}}{\omega_{ms}^{na}}\right)_{Ni}$	$\left(\frac{\omega_{scb}^{na}-\omega_{scb}^{a}}{\omega_{scb}^{na}}\right)_{Ni}$
ω_0	−0.0273	−0.0276	−0.0150	−0.0151

ω_{na} are the resonant frequencies of the 61 atom Cu chain, while ω_a are the resonant frequencies of the 62 atom chain (61 Cu atoms and 1 adsorbate atom).

adsorbates, because of their different bonding energies with the substrate surfaces, cause variations in both mass and stiffness on the resulting adsorbate plus substrate system. The fact that the SCB model is able to predict the different shifts in resonant frequency that occur due to the different
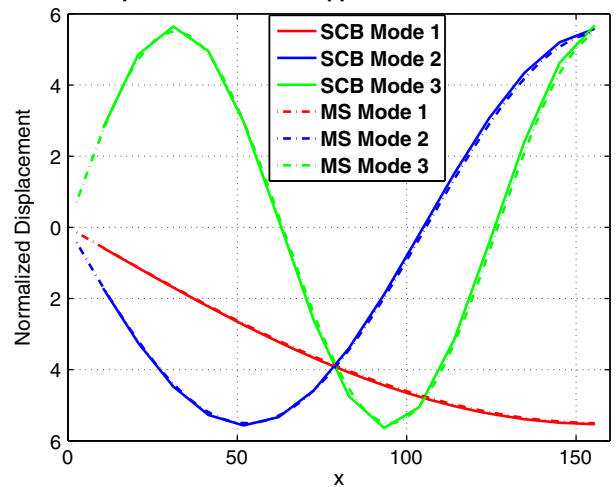
Fig. 10. First three mode shapes for fixed/free copper chain of atoms with a single silver adsorbate atom as calculated using SCB and MS simulations.
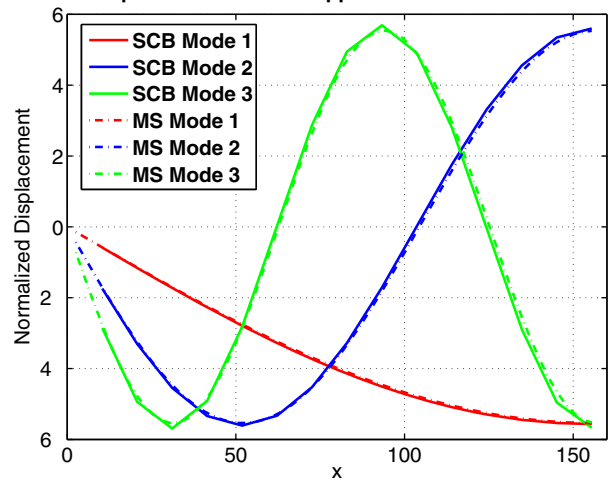
Fig. 11. First three mode shapes for fixed/free copper chain of atoms with a single nickel adsorbate atom as calculated using SCB and MS simulations.

adsorbates indicates its potential in studying nanoscale resonant mass sensing.

The mode shapes of the Cu atomic chain with both Ni and Ag adsorbates are shown in Figs. 10 and 11; we note that the mode shapes and the ordering of the mode shapes is not affected by the adsorbate atom.

6. Conclusions

We have extended the surface Cauchy–Born (SCB) model [48,49] to capture adsorbate/substrate bonding effects between dissimilar materials in order to study the effects of single adsorbate atoms on the resonant frequencies of 1D atomic chains using the finite element method. The key idea was in recognizing that the SCB model cannot, without additional internal degrees of freedom, capture the inhomogeneous surface relaxation that occurs due to interactions of dissimilar materials. Upon incorporation of the internal degrees of freedom, the SCB model was found to accurately capture the minimum energy configurations of the 1D atomic chains under the influence of single adsorbate atoms.

We also demonstrated the ability of the SCB model to capture the resonant frequencies of the 1D atomic chains both with and without the influence of adsorbates. The resonant frequencies were obtained through solution of a standard finite element eigenvalue problem; this underscores one of the distinct advantages of the SCB model, in that it captures surface stress effects originating from undercoordinated surface atoms within a continuum mechanics model. Therefore, the effects of inhomogeneous surface stresses and the resulting deformation due to the adsorbate/substrate interactions are naturally captured by the finite element stiffness matrix, which then shifts the resulting resonant frequencies. The ability to capture the resonant frequency shifts using a finite element solution thus leads to significantly reduced computational costs as compared to a fully atomistic calculation; while the advantages are small in 1D, the computational reduction in higher dimensions will be key, as the solution of fully atomistic eigenvalue problems with tens of millions of degrees of freedom are extremely expensive.

The most important result of this work is that the SCB model was shown to accurately predict the distinct shifts in resonant frequencies of 1D atomic chains due to single adsorbate atoms of different species, and this could be captured in a numerically efficient manner using the finite element method. This predictive ability is critical to nanoscale resonant mass sensing as different adsorbates, due to their distinct masses and bonding energies, will cause unique variations in the resonant frequencies of the substrates on which they are adsorbed. The SCB model is effective because it captures inhomogeneous surface stresses that arise from the bonding of dissimilar materials at an atomistic level, which leads to accurate predictions of resonant frequency shifts due to the adsorption of different materials.

Because of the small surface stresses in 1D, applications to realistic nanoscale mass sensing problems cannot be made without fully 3D calculations, and will be the focus of future research. However, extension of the SCB model to 3D mass sensing should be straight forward, as the SCB model has already been shown to accurately capture surface stress effects on metallic [49] and semiconducting nanowires [72] as compared to benchmark atomistic calculations. In the future, such research, when performed in three-dimensions with realistic interatomic potentials capturing interactions between metallic or semiconducting nanowires and adsorbed atoms and molecules of interest, will enable, among other things, the optimization of the nanowire geometries for maximum sensitivity to the adsorbed mass. Furthermore, the fact that these studies can be performed using finite elements will open new opportunities for nanoscale design engineers.

References

[1] C.M. Lieber, Nanoscale science and technology: building a big future from small things, MRS Bull. 28 (7) (2003) 486–491.
[2] P. Yang, The chemistry and physics of semiconductor nanowires, MRS Bull. 30 (2) (2005) 85–91.
[3] Y. Xia, P. Yang, Y. Sun, Y. Wu, B. Mayers, B. Gates, Y. Yin, F. Kim, H. Yan, One-dimensional nanostructures: synthesis, characterization, and applications, Adv. Mater. 15 (5) (2003) 353–389.
[4] H.G. Craighead, Nanoelectromechanical systems, Science 290 (2000) 1532–1535.
[5] N.V. Lavrik, M.J. Sepaniak, P.G. Datskos, Cantilever transducers as a platform for chemical and biological sensors, Rev. Scientific Inst. 75 (7) (2004) 2229–2253.
[6] K.L. Ekinci, Electromechanical transducers at the nanoscale: actuation and sensing of motion in nanoelectromechanical systems (NEMS), Small 1 (8–9) (2005) 786–797.
[7] J. Lou, L. Tong, Z. Ye, Modeling of silica nanowires for optical sensing, Opt. Exp. 13 (6) (2005) 2135–2140.
[8] Y. Cui, Q. Wei, H. Park, C.M. Lieber, Nanowire nanosensors for highly sensitive and selective detection of biological and chemical species, Science 293 (2001) 1289–1292.
[9] D.W. Carr, S. Evoy, L. Sekaric, H.G. Craighead, J.M. Parpia, Measurement of mechanical resonance and losses in nanometer scale silicon wires, Appl. Phys. Lett. 75 (7) (1999) 920–922.
[10] T.D. Stowe, K. Yasumura, T.W. Kenny, D. Botkin, K. Wago, D. Rugar, Attonewton force detection using ultrathin silicon cantilevers, Appl. Phys. Lett. 71 (2) (1997) 288–290.
[11] J. Yang, T. Ono, M. Esashi, Surface effects and high quality factors in ultrathin single-crystal silicon cantilevers, Appl. Phys. Lett. 77 (23) (2000) 3860–3862.
[12] X. Li, T. Ono, Y. Wang, M. Esashi, Ultrathin single-crystalline-silicon cantilever resonators: fabrication technology and significant specimen size effect on Young's modulus, Appl. Phys. Lett. 83 (15) (2003) 3081–3083.
[13] E.W. Wong, P.E. Sheehan, C.M. Lieber, Nanobeam mechanics: elasticity, strength, and toughness of nanorods and nanotubes, Science 277 (1997) 1971–1975.

[14] S. Cuenot, C. Frétigny, S. Demoustier-Champagne, B. Nysten, Surface tension effect on the mechanical properties of nanomaterials measured by atomic force microscopy, Phys. Rev. B 69 (2004) 165410.

[15] B. Wu, A. Heidelberg, J.J. Boland, Mechanical properties of ultrahigh-strength gold nanowires, Nature Mater. 4 (2005) 525–529.

[16] G.Y. Jing, H.L. Duan, X.M. Sun, Z.S. Zhang, J. Xu, Y.D. Li, J.X. Wang, D.P. Yu, Surface effects on elastic properties of silver nanowires: contact atomic-force microscopy, Phys. Rev. B 73 (2006) 235409.

[17] L.G. Zhou, H. Huang, Are surfaces elastically softer or stiffer? Appl. Phys. Lett. 84 (11) (2004) 1940–1942.

[18] H. Liang, M. Upmanyu, H. Huang, Size-dependent elasticity of nanowires: nonlinear effects, Phys. Rev. B 71 (2005) 241403(R).

[19] R.C. Cammarata, Surface and interface stress effects in thin films, Progr. Surface Sci. 46 (1) (1994) 1–38.

[20] W. Haiss, Surface stress of clean and adsorbate-covered solids, Reports Progress Phys. 64 (2001) 591–648.

[21] M.E. Gurtin, A. Murdoch, A continuum theory of elastic material surfaces, Arch. Rational Mech. Anal. 57 (1975) 291–323.

[22] F.H. Streitz, R.C. Cammarata, K. Sieradzki, Surface-stress effects on elastic properties. I. Thin metal films, Phys. Rev. B 49 (15) (1994) 10699–10706.

[23] R.E. Miller, V.B. Shenoy, Size-dependent elastic properties of nanosized structural elements, Nanotechnology 11 (2000) 139–147.

[24] D.E. Segall, S. Ismail-Beigi, T.A. Arias, Elasticity of nanometer-sized objects, Phys. Rev. B 65 (2002) 214109.

[25] V.B. Shenoy, Atomistic calculations of elastic properties of metallic FCC crystal surfaces, Phys. Rev. B 71 (2005) 094104.

[26] L.H. He, C.W. Lim, B.S. Wu, A continuum model for size-dependent deformation of elastic films of nano-scale thickness, Int. J. Solids Struct. 41 (2004) 847–857.

[27] P. Sharma, S. Ganti, N. Bhate, Effect of surfaces on the size-dependent elastic state of nano-inhomogeneities, Appl. Phys. Lett. 82 (4) (2003) 535–537.

[28] C.T. Sun, H. Zhang, Size-dependent elastic moduli of platelike nanomaterials, J. Appl. Phys. 92 (2) (2003) 1212–1218.

[29] R. Dingreville, J. Qu, M. Cherkaoui, Surface free energy and its effect on the elastic behavior of nano-sized particles, wires and films, J. Mech. Phys. Solids 53 (2005) 1827–1854.

[30] G. Wei, Y. Shouwen, H. Ganyun, Finite element characterization of the size-dependent mechanical behaviour in nanosystems, Nanotechnology 17 (2006) 1118–1122.

[31] J. Wang, H.L. Duan, Z.P. Huang, B.L. Karihaloo, A scaling law for properties of nano-structured materials, Proc. Royal Soc. A 462 (2006) 1355–1363.

[32] E. Tadmor, M. Ortiz, R. Phillips, Quasicontinuum analysis of defects in solids, Philosophical Mag. A 73 (1996) 1529–1563.

[33] L.E. Shilkrot, R.E. Miller, W.A. Curtin, Multiscale plasticity modeling: coupled atomistics and discrete dislocation mechanics, J. Mech. Phys. Solids 52 (2004) 755–787.

[34] J. Fish, W. Chen, Discrete-to-continuum bridging based on multigrid principles, Computer Methods Appl. Mech. Engrg. 193 (2004) 1693–1711.

[35] P.A. Klein, J.A. Zimmerman, Coupled atomistic-continuum simulation using arbitrary overlapping domains, J. Computat. Phys. 213 (2006) 86–116.

[36] F.F. Abraham, J. Broughton, N. Bernstein, E. Kaxiras, Spanning the continuum to quantum length scales in a dynamic simulation of brittle fracture, Europhysics Lett. 44 (1998) 783–787.

[37] R.E. Rudd, J.Q. Broughton, Coarse-grained molecular dynamics and the atomic limit of finite elements, Phys. Rev. B 58 (1998) 5893–5896.

[38] W. E, Z.Y. Huang, A dynamic atomistic-continuum method for the simulation of crystalline materials, J. Computat. Phys. 182 (2002) 234–261.

[39] G.J. Wagner, W.K. Liu, Coupling of atomistic and continuum simulations using a bridging scale decomposition, J. Computat. Phys. 190 (2003) 249–274.

[40] H.S. Park, E.G. Karpov, W.K. Liu, P.A. Klein, The bridging scale for two-dimensional atomistic/continuum coupling, Philosophical Mag. 85 (1) (2005) 79–113.

[41] H.S. Park, E.G. Karpov, W.K. Liu, A temperature equation for coupled atomistic/continuum simulations, Computer Methods Appl. Mech. Engrg. 193 (2004) 1713–1732.

[42] H.S. Park, E.G. Karpov, P.A. Klein, W.K. Liu, Three-dimensional bridging scale analysis of dynamic fracture, J. Computat. Phys. 207 (2005) 588–609.

[43] S.P. Xiao, T. Belytschko, A bridging domain method for coupling continua with molecular dynamics, Computer Methods Appl. Mech. Engrg. 193 (2004) 1645–1669.

[44] W.K. Liu, E.G. Karpov, H.S. Park, Nano Mechanics and Materials: Theory, Multiscale Methods and Applications, John Wiley and Sons, Berlin, 2006.

[45] X. Li, W. E, Multiscale modeling of the dynamics of solids at finite temperature, J. Mech. Phys. Solids 53 (2005) 1650–1685.

[46] W.K. Liu, E.G. Karpov, S. Zhang, H.S. Park, An introduction to computational nano mechanics and materials, Computer Methods Appl. Mech. Engrg. 193 (2004) 1529–1578.

[47] W.A. Curtin, R.E. Miller, Atomistic/continuum coupling in computational materials science, Modell. Simulat. Mater. Sci. Engrg. 11 (2003) R33–R68.

[48] H.S. Park, P.A. Klein, G.J. Wagner, A surface cauchy-born model for nanoscale materials, Int. J. Numer. Methods Engrg. 68 (2006) 1072–1095.

[49] H.S. Park, P.A. Klein, Surface Cauchy–born analysis of surface stress effects on metallic nanowires, Phys. Rev. B 75 (2007) 085408.

[50] Y.T. Yang, C. Callegari, X.L. Feng, K.L. Ekinci, M.L. Roukes, Zeptogram-scale nanomechanical mass sensing, Nano Letters 6 (4) (2006) 583–586.

[51] J. Tamayo, D. Ramos, J. Mertens, M. Calleja, Effects of the adsorbate stiffness on the resonance response of microcantilever sensors, Appl. Phys. Lett. 89 (2006) 224104.

[52] P. Lu, H.P. Lee, C. Lu, S.J. O'Shea, Surface stress effects on the resonance properties of cantilever sensors, Phys. Rev. B 72 (2005) 085405.

[53] P. Lu, F. Shen, S.J. O'Shea, K.H. Lee, T.Y. Ng, Analysis of surface effects on mechanical properties of microcantilevers, Mater. Phys. Mech. 4 (2001) 51–55.

[54] G.Y. Huang, W. Gao, S.W. Yu, Model for the adsorption-induced change in resonance frequency of a cantilever, Appl. Phys. Lett. 89 (2006) 043506.

[55] Q. Ren, Y.P. Zhao, Influence of surface stress on frequency of microcantilever-based biosensors, Microsystem Tech. 10 (2004) 307–314.

[56] M.E. Gurtin, X. Markenscoff, R.N. Thurston, Effects of surface stress on the natural frequency of thin crystals, Appl. Phys. Lett. 29 (9) (1976) 529–530.

[57] H.S. Park, P.A. Klein, Boundary condition and surface stress effects on the resonant properties of metal nanowires, J. Mech. Phys. Solids, submitted.

[58] H.S. Park, J.A. Zimmerman, Modeling inelasticity and failure in gold nanowires, Phys. Rev. B 72 (2005) 054106.

[59] J. Diao, K. Gall, M.L. Dunn, Atomistic simulation of the structure and elastic properties of gold nanowires, J. Mech. Phys. Solids 52 (2004) 1935–1962.

[60] J. Diao, K. Gall, M.L. Dunn, Surface-stress-induced phase transformation in metal nanowires, Nature Mater. 2 (10) (2003) 656–660.

[61] H.S. Park, K. Gall, J.A. Zimmerman, Shape memory and pseudoelasticity in metal nanowires, Phys. Rev. Lett. 95 (2005) 255504.

[62] W. Liang, M. Zhou, F. Ke, Shape memory effect in Cu nanowires, Nano Letters 5 (10) (2005) 2039–2043.

[63] P.A. Klein, A virtual internal bond approach to modeling crack nucleation and growth, Ph.D. Thesis, 1999, Stanford University.

[64] M.S. Daw, M.I. Baskes, Embedded-atom method: derivation and application to impurities, surfaces, and other defects in metals, Phys. Rev. B 29 (12) (1984) 6443–6453.

[65] E.B. Tadmor, G.S. Smith, N. Bernstein, E. Kaxiras, Mixed finite element and atomistic formulation for complex crystals, Phys. Rev. B 59 (1) (1999) 235–245.

[66] Z. Tang, H. Zhao, G. Li, N.R. Aluru, Finite-temperature quasicontinuum method for multiscale analysis of silicon nanostructures, Phys. Rev. B 74 (2006) 064110.

[67] P. Zhang, Y. Huang, P.H. Geubelle, P.A. Klein, K.C. Hwang, The elastic modulus of single-wall carbon nanotubes: a continuum analysis incorporating interatomic potentials, Int. J. Solids Struct. 39 (2002) 3893–3906.

[68] M. Arroyo, T. Belytschko, An atomistic-based finite deformation membrane for single layer crystalline films, J. Mech. Phys. Solids 50 (2002) 1941–1977.

[69] T. Belytschko, W.K. Liu, B. Moran, Nonlinear Finite Elements for Continua and Structures, John Wiley and Sons, 2002.

[70] P.M. Agrawal, B.M. Rice, D.L. Thompson, Predicting trends in rate parameters for self-diffusion on FCC metal surfaces, Surface Sci. 515 (2002) 21–35.

[71] P. Guan, D.R. McKenzie, B.A. Pailthorpe, MD simulations of Ag film growth using the Lennard–Jones potential, J. Phys.-Condensed Matter 8 (1996) 8753–8762.

[72] H.S. Park, P.A. Klein, A surface cauchy-born model for silicon nanostructures, Computer Methods Appl. Mech. Engrg 197 (2008) 3249–3260.